





## Spin-current generation from local spin polarization induced by current through local inversion asymmetry: Double quantum well structure

Yuta Suzuki <sup>1,2</sup>, Yuma Kitagawa <sup>1,2</sup>, Shin-ichiro Tezuka <sup>2</sup>, and Hiroshi Akera <sup>3</sup>

<sup>1</sup>*Division of Applied Physics, Graduate School of Engineering, Hokkaido University, Sapporo, Hokkaido, 060-8628, Japan*

<sup>2</sup>*Sensing Research & Development Department, Innovation Center, Marketing Headquarters, Yokogawa Electric Corporation, Tokyo, 180-8750, Japan*

<sup>3</sup>*Division of Applied Physics, Faculty of Engineering, Hokkaido University, Sapporo, Hokkaido, 060-8628, Japan*



(Received 10 December 2022; revised 1 March 2023; accepted 14 March 2023; published 28 March 2023)

The current-induced spin polarization (CISP) in a system without the inversion symmetry is known to efficiently generate the spin current. In this paper we propose another approach, generating the spin current from the CISP locally arising in a system with the inversion symmetry in the form of the antiparallel CISP in sublattice structure. In this approach the local CISP is extracted from one of sublattices by a selective contact between the sublattice and an electrode. As the simplest system with such antiparallel CISP, we consider a symmetric double-quantum-well structure (DQWS) and calculate the antiparallel CISP and the spin current to a metallic layer in parallel contact with one well of the DQWS using the Boltzmann equation in the relaxation time approximation. When the Fermi energy is large enough that the first-excited sub-band is occupied, the magnitude of the spin current, which is proportional to that of the antiparallel CISP, increases with the interwell tunnel coupling and reaches twice the value of the decoupled quantum well with the broken inversion symmetry. Such an estimate suggests that inversion-symmetric systems can be useful in generating the spin current if the inversion symmetry is locally broken.

DOI: [10.1103/PhysRevB.107.115306](https://doi.org/10.1103/PhysRevB.107.115306)

### I. INTRODUCTION

The spin current plays an important role in spintronics, such as switching the magnetization direction in magnetoresistive random-access memory (MRAM), which is expected to realize ultrahigh density and ultralow power consumption in RAM [1–4]. One way to generate the spin current in non-magnetic materials is to use the diffusion of current-induced spin polarization (CISP) [5–10], which occurs in a system with broken inversion symmetry [11–18]. Such charge-to-spin conversion has been realized experimentally in many systems, such as single-layer quantum wells with a spin-split energy band [11], topological insulators with a spin-momentum locking [12–14], and heterojunctions of atomic layer and metal [16,17].

Recently, the locally broken inversion symmetry in a system with global inversion symmetry has been attracting a lot of attention in superconductivity [19–22] and spintronics [23–36]. The locally broken inversion symmetry exists with the global inversion symmetry if the system has sublattices. In such a system, a pair of spin-degenerate states forms the local spin polarization, which are antiparallel between two sublattices [23–32]. Such antiparallel spin polarization has been theoretically derived [23–25] and experimentally observed in materials such as monolayer PtSe<sub>2</sub> and bilayer WSe<sub>2</sub> by using spin- and angle-resolved photoemission spectroscopy [26–32]. The antiparallel local spin polarization of each spin-degenerate pair gives rise to the antiparallel CISP when contributions from all occupied states are summed in the presence of a charge current [33–36]. It has been shown

that such antiparallel CISP in a sublattice structure can switch the sublattice magnetization of the same structure [33,35,36] for use as memory in antiferromagnetic spintronics [37]. If an efficient generation of the spin current is possible from the antiparallel CISP, it will further enhance the importance of the locally broken inversion symmetry.

In this study, we propose and explore the generation of the spin current from the antiparallel CISP in a sublattice structure with the locally broken inversion symmetry in each sublattice. Our method is to extract the local CISP from one of the sublattices by coupling an electrode selectively to the sublattice. The selective coupling can be achieved, for example, in a two-dimensional (2D) buckled structure such as atomic layer silicene where two sublattices are displaced from each other in the out-of-plane direction.

As a demonstration of the spin current generation from the local CISP, we consider a symmetric double-quantum-well structure (DQWS) [38–46] with the Rashba spin-orbit interaction (SOI) [47–50]. The symmetric DQWS has the inversion symmetry with respect to a point between two wells and exhibits the antiparallel Rashba effective magnetic field, which produces the antiparallel CISP. In this paper we derive an analytical formula for the antiparallel CISP and the spin current to a metallic layer (electrode) in parallel contact with one well of the DQWS by using the Boltzmann equation in the relaxation time approximation. We find that the spin current, which is proportional to the local CISP in the well, increases with the interwell coupling and reaches twice the value at no coupling. The DQWS with no interwell coupling is equivalent

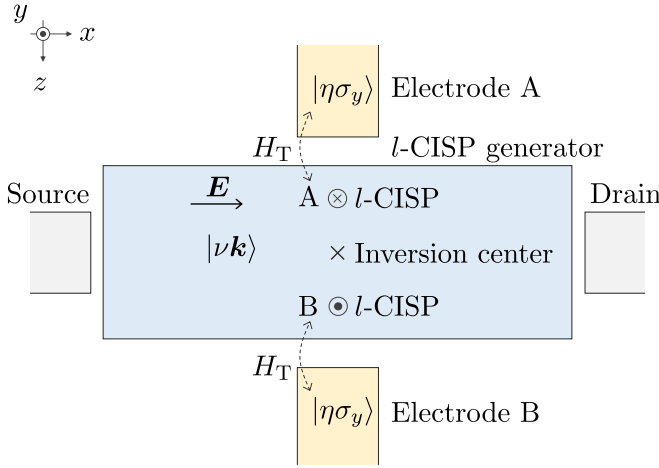


FIG. 1. General model for the generation of the spin current by  $l$ -CISP.

to a pair of isolated quantum wells, each of which has the broken inversion symmetry.

The organization of this paper is as follows. Section II A presents a general scheme for generating the spin current from a system with the locally broken inversion symmetry and introduces the DQWS and atomic layers as examples. Section II B presents the Hamiltonian of a system consisting of the DQWS and electrodes, and describes electronic states in the DQWS and the electrode when the coupling is absent between them. Section III describes the Boltzmann equation for the distribution function generally in a system with the locally broken inversion symmetry in the presence of the in-plane electric field  $E_x$  in the relaxation time approximation, and presents expressions for the antiparallel CISP, the spin current, and the charge current in terms of the distribution function in the first order of  $E_x$ . Section IV presents calculated results in the DQWS. Here we take into account the difference in the electrochemical potential  $\Delta\mu_{ec}$  which appears between the DQWS with  $E_x$  and the electrode in equilibrium. The potential difference  $\Delta\mu_{ec}$  does not produce the spin current, which is proportional to the local value of  $E_x$ . However,  $\Delta\mu_{ec}$  produces the charge current to the electrode, which gives rise to the in-plane spatial variation of  $E_x$  and consequently that of the spin current.

## II. MODEL AND HAMILTONIAN

### A. General model

Figure 1 presents a general model for the generation of the spin current from a system with the inversion symmetry. The model consists of a current-induced local spin polarization ( $l$ -CISP) generator with the inversion symmetry, electrodes A and B for extracting the  $l$ -CISP, and source and drain electrodes. The  $l$ -CISP generator has sublattices (or layers) A and B selectively coupled to the electrodes A and B, respectively. Since the current flows in the  $xy$  plane between the source and drain electrodes, we describe the eigenstate of the  $l$ -CISP generator as  $|\nu\mathbf{k}\rangle$  with the wave vector  $\mathbf{k} = (k_x, k_y)$  and the band index  $\nu$ . The in-plane electric field  $\mathbf{E}$  in the  $l$ -CISP generator induces the  $l$ -CISP, which is antiparallel between

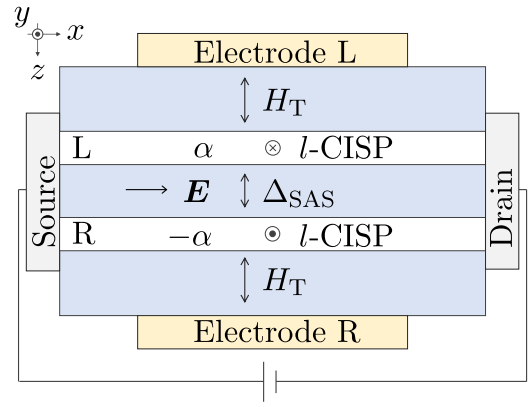


FIG. 2. DQWS model.

A and B sublattices. Here we take the  $y$  axis in the direction of the  $l$ -CISP and choose the eigenstate of the electrode to be the eigenvector of  $\hat{\sigma}_y$  the  $y$  component of the Pauli spin operator, which satisfies  $\hat{\sigma}_y |\sigma_y\rangle = \sigma_y |\sigma_y\rangle$  with  $\sigma_y = \pm 1$ . Such a choice is always possible because we neglect the SOI in the electrodes. Then the eigenstate of the electrode is expressed as  $|\eta\sigma_y\rangle$ , where  $\eta$  represents other quantum numbers. We describe the coupling between the  $l$ -CISP generator and each electrode by the tunneling Hamiltonian  $H_T$ .

Then the Hamiltonian of our general model in Fig. 1 is expressed by

$$H = H_0 + H_{El} + H_T, \quad (1)$$

where  $H_0$  and  $H_{El}$  are the Hamiltonian of the  $l$ -CISP generator and that of the electrodes, respectively. Their eigenvectors satisfy

$$H_0 |\nu\mathbf{k}\rangle = \varepsilon_{\nu\mathbf{k}} |\nu\mathbf{k}\rangle, \quad H_{El} |\xi\eta\sigma_y\rangle = \varepsilon_\eta |\xi\eta\sigma_y\rangle, \quad \xi = A, B \quad (2)$$

where  $\varepsilon_{\nu\mathbf{k}}$  and  $\varepsilon_\eta$  are the corresponding eigenvalues.

We can apply this general model to any inversion-symmetric structure as the  $l$ -CISP generator if the selective coupling is possible between one of sublattices to an electrode. One of such structures, which may be the simplest, is the DQWS in Fig. 2, which we study in subsequent sections. Another important structure is atomic layer. The group IV atomic layer in Fig. 3, for example, has sublattices of A and B sites, which are displaced from each other in the out-of-plane direction, except graphene. Therefore a selective coupling is possible by placing another atomic layer on this buckled atomic layer.

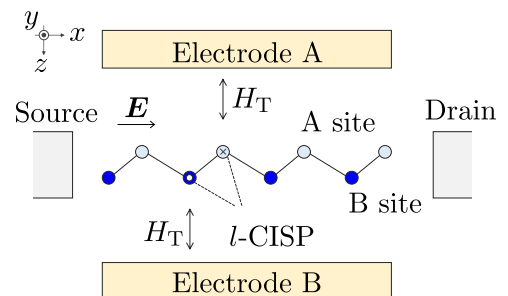


FIG. 3. Atomic layer model.

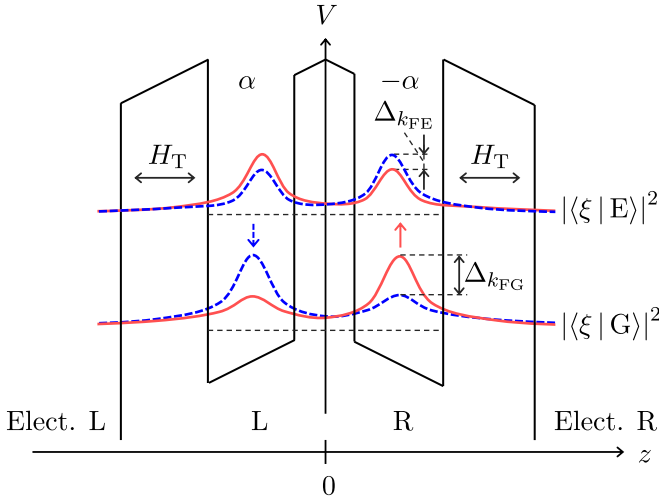


FIG. 4. Potential  $V$  and the local spin polarization in the DQWS in Fig. 2. Solid red and blue dashed lines represent the distribution of spin-up and spin-down states, respectively, at the Fermi energy in the ground sub-band G and the first excited sub-band E. The direction of spin is parallel or antiparallel to the effective magnetic field.  $\Delta_k$  is the magnitude of the local spin polarization at each well ( $\xi = L, R$ ).

### B. Model and Hamiltonian of DQWS

Figure 2 presents a model with the DQWS as the  $l$ -CISP generator, which consists of two wells, L and R, with the Rashba spin-orbit coefficients,  $\alpha(>0)$  and  $-\alpha$ , respectively.  $\Delta_{\text{SAS}}$  is the strength of the coupling between L and R wells. Electrode L and R are selectively coupled to well L and R, respectively. Figure 4 shows the potential and the wave function in the DQWS. The potential has the mirror symmetry with respect to the  $z = 0$  plane. The antiparallel Rashba effective magnetic field is produced by the potential gradient and the band offset [51].

The Hamiltonian of the DQWS is given by

$$H_0 = \frac{\hat{p}_x^2 + \hat{p}_y^2}{2m} + H_{\perp}, \quad (3)$$

where  $\hat{p}_x$  and  $\hat{p}_y$  are the momentum operators and  $m$  is the effective mass of the conduction band. The second term  $H_{\perp}$ , which describes the motion perpendicular to the DQWS, is given by

$$H_{\perp} = -\frac{1}{2}\Delta_{\text{SAS}}\hat{\tau}_1 + \frac{\alpha}{\hbar}\hat{\tau}_3(\hat{p}_y\hat{\sigma}_x - \hat{p}_x\hat{\sigma}_y), \quad (4)$$

where the first term represents the interwell coupling and the second term expresses the antiparallel Rashba effective magnetic field. Here  $\hat{\tau}_\gamma$  ( $\gamma = 1, 2$  and  $3$ ) is the Pauli operator for pseudospin [52,53] defined by

$$\hat{\tau}_1 = |\text{R}\rangle\langle\text{L}| + |\text{L}\rangle\langle\text{R}|, \quad (5)$$

$$\hat{\tau}_2 = i|\text{R}\rangle\langle\text{L}| - i|\text{L}\rangle\langle\text{R}|, \quad (6)$$

$$\hat{\tau}_3 = |\text{L}\rangle\langle\text{L}| - |\text{R}\rangle\langle\text{R}|, \quad (7)$$

where  $|\text{L}\rangle$  and  $|\text{R}\rangle$  represent the lowest bound state in the left and right wells, respectively.

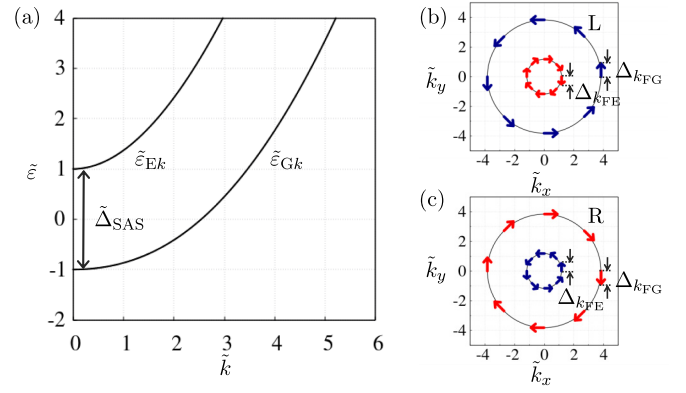


FIG. 5. (a) Sub-band structure in the DQWS at the interwell coupling of  $\tilde{\Delta}_{\text{SAS}} = \Delta_{\text{SAS}}/(2\alpha k_{\text{SO}}) = 2$  with  $k_{\text{SO}} = m\alpha/\hbar^2$ . Dimensionless energy and momentum are defined by  $\tilde{\epsilon} = \epsilon/(2\alpha k_{\text{SO}})$  and  $\tilde{k} = k/k_{\text{SO}}$ , respectively. The local spin polarization is shown by arrows in (b) left and (c) right wells on the Fermi surface at the Fermi energy of  $\tilde{\epsilon}_F = 1.5$ .

The eigenvector is given by  $|n\sigma\mathbf{k}\rangle = |n\rangle|\sigma\rangle|\mathbf{k}\rangle$ . Here  $|\mathbf{k}\rangle$  is the eigenvector of  $\hat{\mathbf{p}} = (\hat{p}_x, \hat{p}_y)$  corresponding to the eigenvalue  $\hbar\mathbf{k}$ . For each  $\mathbf{k}$ ,  $|\sigma\rangle$  is defined by  $\mathbf{e}_b \cdot \hat{\boldsymbol{\sigma}}|\sigma\rangle = \sigma|\sigma\rangle$  where  $\mathbf{e}_b = k^{-1}(k_y, -k_x, 0)$  with  $k = \sqrt{k_x^2 + k_y^2}$  is the unit vector in the direction of the effective magnetic field,  $\hat{\boldsymbol{\sigma}} = (\hat{\sigma}_x, \hat{\sigma}_y, \hat{\sigma}_z)$ , and  $\sigma = \pm 1$ . The vector  $|n\rangle$  ( $n = \pm 1$ ) is given, for each  $\mathbf{k}$  and each  $\sigma$ , by

$$|n\rangle = \frac{1}{\sqrt{2}}(\sqrt{1+n\sigma\Delta_k}|\text{L}\rangle - n\sqrt{1-n\sigma\Delta_k}|\text{R}\rangle), \quad (8)$$

$$\Delta_k = 2\alpha k / \sqrt{\Delta_{\text{SAS}}^2 + (2\alpha k)^2}. \quad (9)$$

The local spin polarization in each well of state  $|n\rangle$  at  $\mathbf{k}$  becomes

$$\sum_{\sigma} \langle n\sigma\mathbf{k} | \hat{\boldsymbol{\sigma}} P_{\xi} | n\sigma\mathbf{k} \rangle = \xi n \Delta_k \mathbf{e}_b, \quad (10)$$

where  $P_{\xi} = |\xi\rangle\langle\xi|$  is the projection operator onto well  $\xi$  ( $\xi = L, R$ ) with  $\xi = 1$  for  $\xi = L$  and  $\xi = -1$  for  $\xi = R$ . Equation (10) shows that the magnitude of the local spin polarization is  $\Delta_k$  and its direction is opposite between  $\xi = L$  and  $R$  and between  $n = -1$  and  $1$ . The eigenvalue of  $H_0$  is given by

$$\varepsilon_{nk} = \frac{\hbar^2 k^2}{2m} + \frac{n}{2} \sqrt{\Delta_{\text{SAS}}^2 + (2\alpha k)^2}, \quad (11)$$

where  $n$  is the sub-band index and we also use  $n = G$  for  $n = -1$  and  $n = E$  for  $n = 1$ , since they are the ground state and the first-excited state, respectively. The eigenvalue has no dependence on  $\sigma$  because the DQWS has the inversion symmetry. The energy difference between the ground and the first-excited states is  $\Delta_{\text{SAS}}$  at  $k = 0$ , while, at  $\Delta_{\text{SAS}} = 0$ , it becomes  $2\alpha k$ , the spin splitting due to the Rashba SOI in a decoupled quantum well. Figure 5(a) presents the eigenenergy as a function of  $k$  and Figs. 5(b) and 5(c) show the local spin polarization [Eq. (10)] in well L and R, respectively, on the Fermi surfaces  $k = k_{\text{FG}}$  ( $n = G$ ) and  $k = k_{\text{FE}}$  ( $n = E$ ).

The Hamiltonian of electrode  $\xi$  ( $=$  L, R) is assumed to be

$$H_{\text{EI}} = \frac{\hat{p}_x^2 + \hat{p}_y^2 + \hat{p}_z^2}{2m_{\text{EI}}} + \varepsilon_0. \quad (12)$$

Here the effective mass  $m_{\text{EI}}$  is the same in  $\xi =$  L and R, and  $\varepsilon_0$  ( $< 0$ ) is the energy at the band bottom. The eigenvector is  $|\xi k k_z \sigma_y\rangle$ , and the eigenenergy is

$$\varepsilon_{k k_z} = \frac{\hbar^2(k^2 + k_z^2)}{2m_{\text{EI}}} + \varepsilon_0. \quad (13)$$

The tunneling Hamiltonian is given by

$$H_{\text{T}} = \sum_{\xi k k_z \sigma_y} |\xi k \sigma_y\rangle \langle \xi k \sigma_y | H_{\text{T}} | \xi k k_z \sigma_y\rangle \langle \xi k k_z \sigma_y | + \text{H.c.}, \quad (14)$$

where  $|\xi k \sigma_y\rangle = |\xi \rangle |k\rangle | \sigma_y\rangle$  and H.c. denotes the Hermitian conjugate of the preceding term. Here we have assumed that  $H_{\text{T}}$  has the in-plane translational symmetry and does not include the spin and that the tunneling occurs between the electrode and the well in the same side. The matrix element  $\langle \xi k \sigma_y | H_{\text{T}} | \xi k k_z \sigma_y\rangle$  is then independent of  $\mathbf{k}$  and  $\sigma_y$ , and is assumed to be the same in  $\xi =$  L and R.

With use of  $H_{\text{T}}$ , we express the rate of the transition between  $|n\sigma k\rangle$  and  $|\xi k k_z \sigma_y\rangle$  at the same energy ( $\varepsilon_{nk} = \varepsilon_{k k_z}$ ) in Eq. (31). The value of  $k_z$ , satisfying  $\varepsilon_{nk} = \varepsilon_{k k_z} = \hbar^2(k^2 + k_z^2)/(2m_{\text{EI}}) + \varepsilon_0$ , varies depending on  $n$  and  $k$ . However, we neglect the variation of  $\langle \xi k \sigma_y | H_{\text{T}} | \xi k k_z \sigma_y\rangle$  with  $k_z$  by choosing a sufficiently large value of  $|\varepsilon_0|$  such that  $|\varepsilon_0| \gg \varepsilon_{\text{F}}$  ( $\varepsilon_{\text{F}}$ : the Fermi energy of the DQWS). This is because the variation of  $k_z$  is of the order of  $k_z \varepsilon_{\text{F}}/|\varepsilon_0|$  from  $\hbar^2 k_z^2/(2m_{\text{EI}}) = -\varepsilon_0 - \hbar^2 k^2/(2m_{\text{EI}}) + \varepsilon_{nk} = -\varepsilon_0 + O(\varepsilon_{\text{F}})$ .

### III. CALCULATION METHOD AND FORMULAS

We calculate the  $l$ -CISP, the spin current, and the charge current by employing the Boltzmann equation in the first order of  $\mathbf{E}$ . We assume that spatial variations of  $\mathbf{E}$  and the potential  $\phi$  are in the length scale much longer than the mean-free path. Then using local values of  $\mathbf{E}$  and  $\phi$ , the steady-state Boltzmann equation for the distribution function  $f_{\nu k}$  (of the general model in Sec. II A) with  $\mathbf{k}$  the in-plane wave vector and  $\nu$  the band index is given, in the relaxation time approximation with the momentum relaxation time  $\tau_p$ , by

$$\frac{(-e)\mathbf{E}}{\hbar} \cdot \frac{\partial f_{\nu k}}{\partial \mathbf{k}} = -\frac{f_{\nu k} - f_0(\varepsilon_{\nu k} - e\phi, \mu_{\text{ec}})}{\tau_p}, \quad (15)$$

where  $e$  ( $> 0$ ) is the absolute value of the electronic charge and  $f_0(\varepsilon, \mu_{\text{ec}}) = \{\exp[(\varepsilon - \mu_{\text{ec}})/k_{\text{B}}T] + 1\}^{-1}$  with  $\mu_{\text{ec}}$  the electrochemical potential,  $k_{\text{B}}$  the Boltzmann constant, and  $T$  the temperature. The distribution function is decomposed into the equilibrium distribution and the deviation  $f_{\nu k}^{(1)}$  in the first order of  $\mathbf{E}$ :

$$f_{\nu k} = f_0(\varepsilon_{\nu k} - e\phi, \mu_{\text{ec}}) + f_{\nu k}^{(1)}, \quad (16)$$

in which  $f_{\nu k}^{(1)}$  is obtained, from Eq. (15), to be

$$f_{\nu k}^{(1)} = \frac{\tau_p e \mathbf{E} \cdot \mathbf{k}}{\hbar k} \frac{\partial f_0}{\partial k}. \quad (17)$$

With use of  $f_{\nu k}^{(1)}$ , the  $l$ -CISP per unit area,  $\sigma_{\xi} = (\sigma_{\xi x}, \sigma_{\xi y}, \sigma_{\xi z})$ , in sub-band (or layer)  $\xi$  is given by

$$\sigma_{\xi} = \frac{1}{S} \sum_{\nu k} f_{\nu k}^{(1)} \langle \nu k | \hat{\sigma} P_{\xi} | \nu k \rangle, \quad (18)$$

with  $S$  the system area.

Spin and charge currents per unit area,  $j_{z,\xi}^{\text{s}}$  and  $j_{z,\xi}^{\text{c}}$ , into electrode  $\xi$  are given by

$$j_{z,\xi}^{\text{s}} = \frac{\hbar}{2} (j_{z,\xi}^{\uparrow} - j_{z,\xi}^{\downarrow}), \quad (19)$$

$$j_{z,\xi}^{\text{c}} = -e(j_{z,\xi}^{\uparrow} + j_{z,\xi}^{\downarrow}), \quad (20)$$

where  $j_{z,\xi}^{\sigma_y}$  ( $\sigma_y = \uparrow, \downarrow$ ) is the number current per unit area of spin-up and spin-down electrons into electrode  $\xi$  and is given by

$$j_{z,\xi}^{\sigma_y} = \frac{1}{S} \sum_{\nu k} \sum_{\eta} W_{\xi \eta \sigma_y, \nu k} [f_{\nu k} - f_0(\varepsilon_{\eta}, \mu_{\text{ec}}^{\text{eq}})], \quad (21)$$

where we assumed that electrodes are in equilibrium with the electrochemical potential  $\mu_{\text{ec}}^{\text{eq}}$  and the temperature  $T$ . The tunneling rate between the  $l$ -CISP generator and electrode  $\xi$ ,  $W_{\xi \eta \sigma_y, \nu k}$ , is given by

$$W_{\xi \eta \sigma_y, \nu k} = \frac{2\pi}{\hbar} |\langle \xi \eta \sigma_y | H_{\text{T}} | \nu k \rangle|^2 \delta(\varepsilon_{\nu k} - e\phi - \varepsilon_{\eta}). \quad (22)$$

The charge current density in the  $l$ -CISP generator,  $\mathbf{j}^{\text{c}} = (j_x^{\text{c}}, j_y^{\text{c}})$ , is expressed by

$$\mathbf{j}^{\text{c}} = \frac{-e}{S} \sum_{\nu k} f_{\nu k} \left( \frac{1}{\hbar} \frac{\partial \varepsilon_{\nu k}}{\partial \mathbf{k}} \right). \quad (23)$$

### IV. CALCULATED RESULTS IN DQWS

#### A. Antiparallel CISP

The  $l$ -CISP in well  $\xi$  of the DQWS becomes, by applying Eq. (18) to the DQWS and substituting the local spin polarization in Eq. (10),

$$\sigma_{\xi} = \frac{1}{S} \sum_{n\sigma k} f_{n\sigma k}^{(1)} \langle n\sigma k | \hat{\sigma} P_{\xi} | n\sigma k \rangle = \frac{\xi}{S} \sum_{nk} f_{nk}^{(1)} n \Delta_k \mathbf{e}_b, \quad (24)$$

where  $n$  takes either  $n = -1, 1$  or  $n = \text{G, E}$ . By choosing  $\mathbf{E} = (E_x, 0, 0)$ ,  $\sigma_{\xi}$  is in the  $y$  direction because  $f_{nk}^{(1)} = k_x g(k)$  for  $\mathbf{E} = (E_x, 0, 0)$  and  $\mathbf{e}_b = k^{-1}(k_y, -k_x, 0)$ . At  $T = 0$ , the  $l$ -CISP is obtained to be

$$\sigma_{\text{L}y} = -\sigma_{\text{R}y} = \frac{e E_x \tau_p}{4\pi \hbar} \sum_n n k_{\text{Fn}} \Delta_{k_{\text{Fn}}}. \quad (25)$$

Figure 6 presents the dependence of  $\sigma_{\text{L}y}$  on the Fermi energy  $\varepsilon_{\text{F}}$  at fixed values of the interwell coupling,  $\Delta_{\text{SAS}}/(2\alpha k_{\text{SO}}) = 0, 2, 5$ , and  $10$  ( $k_{\text{SO}} = m\alpha \hbar^{-2}$ ). At  $\Delta_{\text{SAS}} = 0$ ,  $\sigma_{\text{L}y}$  reduces to the CISP in a single QW and is given in  $\varepsilon_{\text{F}} > 0$  by  $\sigma_{y0} = -e E_x \tau_p k_{\text{SO}}/(2\pi \hbar)$  with no dependence on  $\varepsilon_{\text{F}}$ . With respect to the  $\varepsilon_{\text{F}}$  dependence of  $\sigma_{\text{L}y}$ , we focus on the region of  $\Delta_{\text{SAS}} \geq 2\alpha k_{\text{SO}}$  where  $\varepsilon_{nk}$  becomes a monotonically increasing function of  $k$  as shown in Fig. 5(a). In the

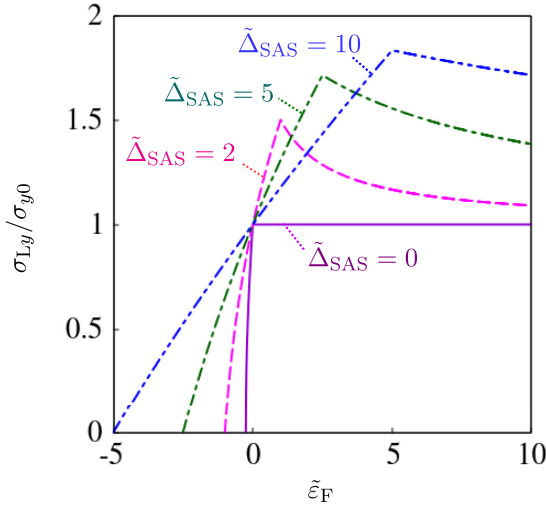


FIG. 6. The dependence of the *l*-CISP  $\sigma_{Ly}$  on the Fermi energy  $\varepsilon_F$  and the interwell coupling  $\Delta_{SAS}$ . Dimensionless parameters are defined by  $\tilde{\varepsilon}_F = \varepsilon_F/(2\alpha k_{SO})$  and  $\tilde{\Delta}_{SAS} = \Delta_{SAS}/(2\alpha k_{SO})$ .  $\sigma_{y0} = -eE_x \tau_p k_{SO}/(2\pi\hbar)$  is the value at  $\Delta_{SAS} = 0$  in  $\varepsilon_F > 0$ . In a typical semiconductor DQWS,  $\varepsilon_F \sim 10$  meV and  $\Delta_{SAS} < 3$  meV [54–56].

lower-energy region of  $-\Delta_{SAS}/2 < \varepsilon_F < \Delta_{SAS}/2$  where only the ground sub-band is occupied by electrons, Eq. (25) becomes  $\sigma_{Ly} = -(4\pi\hbar)^{-1}eE_x \tau_p k_{FG} \Delta_{k_{FG}}$  which increases with  $\varepsilon_F$ . In  $\varepsilon_F > \Delta_{SAS}/2$ , on the other hand, the contribution from the first-excited sub-band suppresses  $\sigma_{Ly}$ , which decreases with  $\varepsilon_F$  and approaches  $\sigma_{y0}$  in the limit of  $\varepsilon_F \rightarrow \infty$ . Thus  $\sigma_{Ly}$  exhibits the maximum at  $\varepsilon_F = \Delta_{SAS}/2$ , the value of which is  $\sigma_{Ly} = 2\sigma_{y0}(\Delta_{SAS} + 2\alpha k_{SO})/(\Delta_{SAS} + 4\alpha k_{SO})$ .

Figure 7 shows the dependence of  $\sigma_{Ly}$  on the interwell coupling  $\Delta_{SAS}$  at fixed values of the Rashba coefficient,  $2\alpha k_F/\varepsilon_F = 0.2, 0.3$ , and  $0.5$  ( $k_F = \sqrt{2m\varepsilon_F}/\hbar$ ), in the region

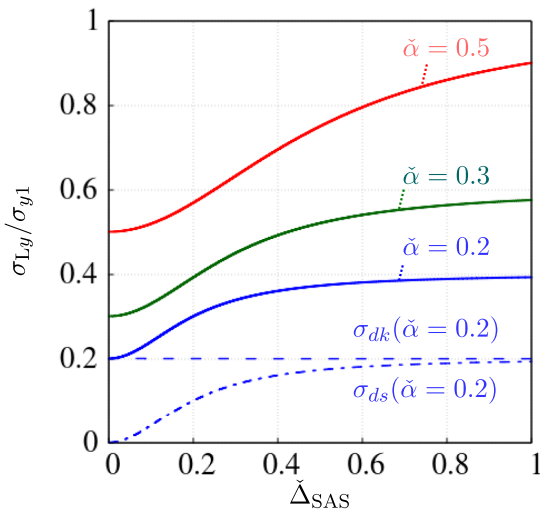


FIG. 7. The dependence of the *l*-CISP  $\sigma_{Ly}$  on the interwell coupling  $\Delta_{SAS}$  and the Rashba coefficient  $\alpha$  in  $\varepsilon_F > \Delta_{SAS}/2$  where both the ground and the first-excited sub-bands are occupied.  $\tilde{\Delta}_{SAS} = \Delta_{SAS}/\varepsilon_F$ ,  $\tilde{\alpha} = 2\alpha k_F/\varepsilon_F$  ( $k_F = \sqrt{2m\varepsilon_F}/\hbar$ ), and  $\sigma_{y1} = \sigma_{y0}/\tilde{\alpha} = -eE_x \tau_p k_F/(8\pi\hbar)$ . Dashed and dash-dotted lines plot  $\sigma_{dk}$  [Eq.(28)] and  $\sigma_{ds}$  [Eq. (29)], respectively, at  $\tilde{\alpha} = 0.2$ .

of  $\varepsilon_F > \Delta_{SAS}/2$  in which both the ground and the first-excited sub-bands contribute to  $\sigma_{Ly}$ . We find that  $\Delta_{SAS}$  enhances  $\sigma_{Ly}$ . Since  $k_{Fn}$  in Eq. (25) is given in  $\varepsilon_F > \Delta_{SAS}/2$  by  $k_{Fn} = \sqrt{k_F^2 + 2k_{SO}^2 - nm\hbar^{-2} \sqrt{\Delta_{SAS}^2 + (2\alpha k_F)^2 + (2\alpha k_{SO})^2}}$ ,  $\sigma_{Ly}$  becomes

$$\sigma_{Ly} = \sigma_{y0} \left( 1 + \frac{\Delta_{SAS}^2}{\Delta_{SAS}^2 + (2\alpha k_F)^2} \right), \quad (26)$$

which indicates that  $\sigma_{Ly}$  increases from  $\sigma_{y0}$  at  $\Delta_{SAS} = 0$  to  $2\sigma_{y0}$  in the limit of  $\Delta_{SAS}/(2\alpha k_F) \rightarrow \infty$ . This enhancement originates from the increasing difference in the local spin polarization  $\Delta_k$  between the ground and the first-excited sub-bands at the Fermi energy. To show this, we divide Eq. (25) into two terms

$$\sigma_{Ly} = \sigma_{dk} + \sigma_{ds}, \quad (27)$$

with

$$\begin{aligned} \sigma_{dk} &= -\frac{eE_x \tau_p}{8\pi\hbar} (k_{FG} - k_{FE})(\Delta_{k_{FG}} + \Delta_{k_{FE}}) \\ &= \sigma_{y0} \frac{\Delta_{SAS}^2 + 2(\alpha k_F)^2 \left[ 1 + \sqrt{1 - \Delta_{SAS}^2/(4\varepsilon_F^2)} \right]}{\Delta_{SAS}^2 + (2\alpha k_F)^2}, \end{aligned} \quad (28)$$

$$\begin{aligned} \sigma_{ds} &= -\frac{eE_x \tau_p}{8\pi\hbar} (k_{FG} + k_{FE})(\Delta_{k_{FG}} - \Delta_{k_{FE}}) \\ &= \sigma_{y0} \frac{\Delta_{SAS}^2 + 2(\alpha k_F)^2 \left[ 1 - \sqrt{1 - \Delta_{SAS}^2/(4\varepsilon_F^2)} \right]}{\Delta_{SAS}^2 + (2\alpha k_F)^2}. \end{aligned} \quad (29)$$

The  $\Delta_{SAS}$  dependence of  $\sigma_{dk}$  and that of  $\sigma_{ds}$  at  $2\alpha k_F/\varepsilon_F = 0.2$  are indicated by dashed and dash-dotted lines in Fig. 7. These plots show that the twofold increase of  $\sigma_{Ly}$  with  $\Delta_{SAS}$  is given by the increase of  $\sigma_{ds}$ , which in turn is given by the increase of  $\Delta_{k_{FG}} - \Delta_{k_{FE}}$ . Therefore the twofold increase of  $\sigma_{Ly}$  originates from the  $k$  dependence of the local spin polarization  $\Delta_k$ , which is unique to a system with the locally broken inversion symmetry. As derived from Eqs. (28) and (29),  $\sigma_{dk} = \sigma_{y0}$  and  $\sigma_{ds} = 0$  at  $\Delta_{SAS} = 0$  and  $\sigma_{dk} = \sigma_{ds} = \sigma_{y0}$  at  $\Delta_{SAS}/(2\alpha k_F) \rightarrow \infty$ .

## B. Spin current

We calculate the spin current and the charge current by considering two driving forces, the in-plane electrical field  $\mathbf{E}$  and the electrochemical potential difference between the DQWS and the electrode  $\Delta\mu_{ec} = \mu_{ec} - \mu_{ec}^{eq} = -e\phi$ . By applying Eqs. (19), (21), and (22) to the DQWS model, the spin current to electrode  $\xi$  is given by

$$j_{z,\xi}^s = \frac{1}{S} \sum_{\sigma_y} \frac{\hbar\sigma_y}{2} \sum_{n\sigma k} \sum_{k_z} W_{n\sigma k, \xi k k_z \sigma_y} [f_{nk} - f_0(\varepsilon_{kk_z}, \mu_{ec}^{eq})], \quad (30)$$

with

$$W_{n\sigma k, \xi k k_z \sigma_y} = \frac{2\pi}{\hbar} |\langle n\sigma k | H_T | \xi k k_z \sigma_y \rangle|^2 \delta(\varepsilon_{nk} - e\phi - \varepsilon_{kk_z}), \quad (31)$$



and is expressed as

$$j_{z,\xi}^s = \frac{1}{S} \sum_{\sigma_y} \frac{\hbar \sigma_y}{2} \sum_{n\sigma k} |\langle n\sigma k | \xi k \sigma_y \rangle|^2 \times \frac{1}{\tau_\xi} [f_{nk} - f_0(\varepsilon_{nk} - e\phi, \mu_{ec}^{eq})], \quad (32)$$

with  $\tau_\xi$ , the lifetime of state  $|\xi k \sigma_y\rangle$  due to tunneling to electrode  $\xi$ , defined by

$$\frac{1}{\tau_\xi} = \sum_{k_z} \frac{2\pi}{\hbar} |\langle \xi k \sigma_y | \hat{H}_T | \xi k k_z \sigma_y \rangle|^2 \delta(\varepsilon_{nk} - e\phi - \varepsilon_{k k_z}). \quad (33)$$

Since the matrix element  $\langle \xi k \sigma_y | \hat{H}_T | \xi k k_z \sigma_y \rangle$  has no dependences on  $\xi$ ,  $\mathbf{k}$ , and  $\sigma_y$  and a negligible dependence on  $k_z$  owing to the assumptions made in Sec. II B,  $\tau_\xi^{-1}$  is proportional to the density of states, whose dependence on  $\varepsilon_{nk} - e\phi$  is also negligible owing to the assumption of  $|\varepsilon_0| \gg \varepsilon_F$  (Sec. II B). Then we obtain

$$j_{z,\xi}^s = j_{z,\xi}^E + j_{z,\xi}^{S\mu_{ec}}, \quad (34)$$

with

$$j_{z,\xi}^E = \frac{\hbar}{2\tau_\xi S} \sum_{n\sigma k} f_{nk}^{(1)} \langle n\sigma k | \hat{\sigma}_y P_\xi | n\sigma k \rangle, \quad (35)$$

$$j_{z,\xi}^{S\mu_{ec}} = \frac{\hbar}{2\tau_\xi S} \Delta\mu_{ec} \frac{\partial}{\partial \mu_{ec}} \sum_{n\sigma k} f_0(\varepsilon_{nk}, \mu_{ec}^{eq}) \langle n\sigma k | \hat{\sigma}_y P_\xi | n\sigma k \rangle, \quad (36)$$

where  $j_{z,\xi}^E$  and  $j_{z,\xi}^{S\mu_{ec}}$  are components driven by  $\mathbf{E}$  and  $\Delta\mu_{ec}$ , respectively. Since  $f_0(\varepsilon_{nk}, \mu_{ec}^{eq})$ , an isotropic distribution in  $\mathbf{k}$  space, does not produce the spin polarization, we have  $j_{z,\xi}^{S\mu_{ec}} = 0$  and obtain

$$j_{z,\xi}^s = \frac{\hbar}{2\tau_\xi} \sigma_{\xi y}. \quad (37)$$

We find that the spin current is proportional to the  $l$ -CISP  $\sigma_{\xi y}$  driven by  $E_x$ , and is not produced by  $\Delta\mu_{ec}$ .

### C. Spatial variations

The electrochemical potential difference  $\Delta\mu_{ec} = -e\phi$ , however, produces the charge current to electrodes, which in turn gives rise to the spatial variation of  $E_x$  and consequently that of the spin current. We calculate such spatial variations with Kirchhoff's first law.

The charge current densities  $j_{z,\xi}^c(x)$  [Eq. (20)] and  $j_x^c(x)$  [Eq. (23)] are given by

$$j_{z,L}^c = j_{z,R}^c = g_0 \phi(x), \quad j_x^c = \sigma_0 E_x(x), \quad (38)$$

where  $g_0$  is the conductance between the DQWS and each electrode per unit area and  $\sigma_0$  is the electrical conductivity of the DQWS. Kirchhoff's first law, applied to the area of the DQWS with width  $dx$  and unit length, gives

$$j_x^c(x) - j_x^c(x+dx) - [j_{z,L}^c(x) + j_{z,R}^c(x)]dx = 0, \quad (39)$$

which leads to

$$\frac{d^2\phi(x)}{dx^2} - \frac{\phi(x)}{\lambda^2} = 0, \quad \lambda = \sqrt{\sigma_0/2g_0}, \quad (40)$$

where  $\lambda$  represents the length scale of the variation. By imposing the zero net current to each electrode  $\int j_{z,\xi}^c(x)dx = 0$ , we obtain  $\phi(x)$  and  $E_x(x)$  to be

$$\phi(x) = -\frac{\Delta\phi}{2} \frac{\sinh(x/\lambda)}{\sinh(L_e/2\lambda)}, \quad (41)$$

$$E_x(x) = \frac{\Delta\phi}{2\lambda} \frac{\cosh(x/\lambda)}{\sinh(L_e/2\lambda)}, \quad (42)$$

where  $\Delta\phi$  is the voltage drop across the electrode length  $L_e$ . Figure 8(a) shows a schematic view of spatial variations of the spin current  $j_z^s$ , the charge currents  $j_z^c$ , and  $j_x^c$ . The spin current  $j_z^s(x)$  and  $E_x(x)$  are the smallest at the electrode center ( $x = 0$ ) because the charge current flows out to electrodes in  $x < 0$  and flows in to the DQWS in  $x > 0$ . Figure 8(b) and 8(c) present the  $\lambda$  dependence of  $E_x(x)$  and  $\phi(x)$ . As shown in Eq. (39),  $\lambda$  is longer when the DQWS has a higher conductivity and junctions to electrodes have a lower conductance. Since the spin current at each  $x$  is proportional to  $E_x(x)$ , the total spin current to each electrode is determined by  $\Delta\phi$ , the potential drop in the electrode length.

## V. CONCLUSIONS

We have proposed the generation of the spin current from the antiparallel CISP, which occurs in a system with the locally broken inversion symmetry, by selectively coupling an electrode to one of sublattices (or layers) with the local CISP. Since a variety of materials and systems have the locally broken inversion symmetry, we expect that our proposal could enhance the possibility of finding an efficient spin current source. Especially, atomic layer materials with sublattices displaced from each other in the out-of-plane direction are promising candidates in that the selective coupling can be implemented by simply placing another layer as the electrode onto the layer with the antiparallel CISP.

We have demonstrated generating the spin current from the antiparallel CISP in a system consisting of the DQWS and electrodes as the simplest example. We have calculated the antiparallel CISP in the DQWS using the Boltzmann equation in the relaxation time approximation, and found, in the large Fermi energy region with the first-excited sub-band occupied, that the magnitude of the antiparallel CISP increases by two when the interwell coupling is increased from no coupling (decoupled quantum wells with broken inversion symmetry) to a strong coupling, even though the local spin polarization of the spin-degenerate eigenstate pair decreases with the interwell coupling. This twofold increase originates from the momentum dependence of the local spin polarization, which is unique to the system with the locally broken inversion symmetry. Such interwell-coupling dependence of the antiparallel CISP is reflected in the spin current to each electrode because the spin current is proportional to the local CISP in one well, to which the electrode is coupled, as long as tunneling rates to the electrode are approximately the same in all eigenstates occupied in the DQWS.

The spin current generation from the antiparallel CISP in DQWS, in which the charge current along  $x$  induces the spin polarization along  $y$  to flow along  $z$ , can be regarded as a spin Hall effect [57–61] and categorized as the intrinsic spin Hall effect [59,60] because it originates from the band structure and

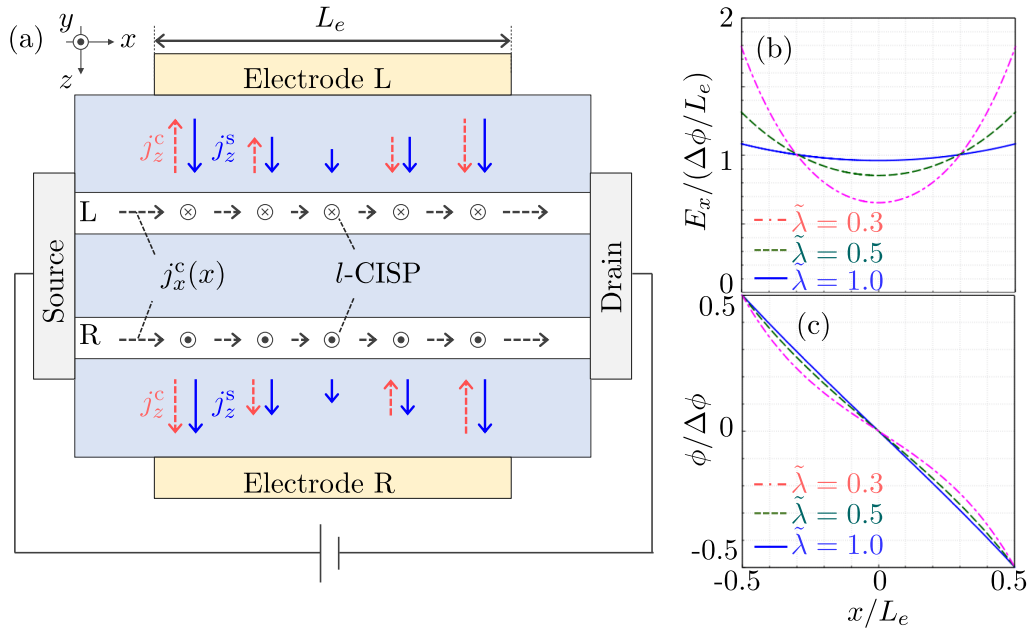


FIG. 8. (a) Schematic view of spatial variations of the spin current  $j_z^s$  (blue solid arrow), the charge current  $j_z^c$  (red dashed), and  $j_x^c$  (black dashed).  $L_e$  is the electrode length. Spatial variations of (b)  $E_x(x)$  and (c)  $\phi(x)$  are presented for  $\tilde{\lambda} = \lambda/L_e = 0.3, 0.5,$  and  $1.0$ .

the spin polarization of each eigenstate. In the spin Hall effect in the bulk, the charge current first produces the spin current, which then accumulates the antiparallel spin polarization on opposite surfaces. On the other hand, in the present DQWS, the charge current first induces the antiparallel spin polarization in two wells, which then generates the spin current by diffusing into electrodes. It has a close correspondence with the spin current generation from 3D topological insulators in which opposite surfaces exhibit antiparallel CISP [12–14]. However, the present DQWS, as we have demonstrated in this

paper, has a unique feature brought by the interwell coupling, which is absent in 3D topological insulators with decoupled surfaces.

#### ACKNOWLEDGMENTS

This work was partly supported by Grant-in-Aid for Scientific Research (C) Grant No. JP21K03413 from the Japan Society for the Promotion of Science (JSPS).

- [1] I. Žutić, J. Fabian, and S. D. Sarma, Spintronics: Fundamentals and applications, *Rev. Mod. Phys.* **76**, 323 (2004).
- [2] A. Chernyshov, M. Overby, X. Liu, J. K. Furdyna, Y. Lyanda-Geller, and L. P. Rokhinson, Evidence for reversible control of magnetization in a ferromagnetic material by means of spin-orbit magnetic field, *Nat. Phys.* **5**, 656 (2009).
- [3] T. Liu, X. Wang, H. Wang, G. Shi, F. Gao, H. Feng, H. Deng, L. Hu, E. Lochner, P. Schlottmann, S. von Molnár, Y. Li, J. Zhao, and P. Xiong, Linear and nonlinear two-terminal spin-valve effect from chirality-induced spin selectivity, *ACS Nano* **14**, 15983 (2020).
- [4] H. Wu, A. Chen, P. Zhang, H. He, J. Nance, C. Guo, J. Sasaki, T. Shirokura, P. N. Hai, B. Fang, S. A. Razavi, K. Wong, Y. Wen, Y. Ma, G. Yu, G. P. Carman, X. Han, X. Zhang, and K. L. Wang, Magnetic memory driven by topological insulators, *Nat. Commun.* **12**, 6251 (2021).
- [5] V. Edelstein, Spin polarization of conduction electrons induced by electric current in two-dimensional asymmetric electron systems, *Solid State Commun.* **73**, 233 (1990).
- [6] V. K. Kalevich and V. L. Korenev, Effect of electric field on the optical orientation of 2D electrons, *JETP Lett.* **52**, 230 (1990).
- [7] A. Y. Silov, P. A. Blajnov, J. H. Wolter, R. Hey, K. H. Ploog, and N. S. Averkiev, Current-induced spin polarization at a single heterojunction, *Appl. Phys. Lett.* **85**, 5929 (2004).
- [8] Y. K. Kato, R. C. Myers, A. C. Gossard, and D. D. Awschalom, Current-Induced Spin Polarization in Strained Semiconductors, *Phys. Rev. Lett.* **93**, 176601 (2004).
- [9] C. L. Yang, H. T. He, L. Ding, L. J. Cui, Y. P. Zeng, J. N. Wang, and W. K. Ge, Spectral Dependence of Spin Photocurrent and Current-Induced Spin Polarization in an InGaAs/InAlAs Two-Dimensional Electron Gas, *Phys. Rev. Lett.* **96**, 186605 (2006).
- [10] M. Trushin and J. Schliemann, Anisotropic current-induced spin accumulation in the two-dimensional electron gas with spin-orbit coupling, *Phys. Rev. B* **75**, 155323 (2007).
- [11] Y. Wang, R. Ramaswamy, M. Motapothula, K. Narayanapillai, D. Zhu, J. Yu, T. Venkatesan, and H. Yang, Room-temperature giant charge-to-spin conversion at the SrTiO<sub>3</sub>-LaAlO<sub>3</sub> oxide interface, *Nano Lett.* **17**, 7659 (2017).

- [12] A. R. Mellnik, J. S. Lee, A. Richardella, J. L. Grab, P. J. Mintun, M. H. Fischer, A. Vaezi, A. Manchon, E.-A. Kim, N. Samarth, and D. C. Ralph, Spin-transfer torque generated by a topological insulator, *Nature (London)* **511**, 449 (2014).
- [13] K. Kondou, R. Yoshimi, A. Tsukazaki, Y. Fukuma, J. Matsuno, K. S. Takahashi, M. Kawasaki, Y. Tokura, and Y. Otani, Fermi-level-dependent charge-to-spin current conversion by Dirac surface states of topological insulators, *Nat. Phys.* **12**, 1027 (2016).
- [14] K. Kondou, H. Tsai, H. Isshiki, and Y. Otani, Efficient spin current generation and suppression of magnetic damping due to fast spin ejection from nonmagnetic metal/indium-tin-oxide interfaces, *APL Mater.* **6**, 101105 (2018).
- [15] M. B. Jungfleisch, W. Zhang, J. Sklenar, W. Jiang, J. E. Pearson, J. B. Ketterson, and A. Hoffmann, Interface-driven spin-torque ferromagnetic resonance by Rashba coupling at the interface between nonmagnetic materials, *Phys. Rev. B* **93**, 224419 (2016).
- [16] Q. Shao, G. Yu, Y.-W. Lan, Y. Shi, M.-Y. Li, C. Zheng, X. Zhu, L.-J. Li, P. K. Amiri, and K. L. Wang, Strong Rashba-Edelstein effect-induced spin-orbit torques in monolayer transition metal dichalcogenide/ferromagnet bilayers, *Nano Lett.* **16**, 7514 (2016).
- [17] Y. Liu and Q. Shao, Two-dimensional materials for energy-efficient spin-orbit torque devices, *ACS Nano* **14**, 9389 (2020).
- [18] S. Karube, N. Tezuka, M. Kohda, and J. Nitta, Anomalous Spin-Orbit Field via the Rashba-Edelstein Effect at the W/Pt Interface, *Phys. Rev. Appl.* **13**, 024009 (2020).
- [19] M. H. Fischer, F. Loder, and M. Sigrist, Superconductivity and local noncentrosymmetry in crystal lattices, *Phys. Rev. B* **84**, 184533 (2011).
- [20] D. Maruyama, M. Sigrist, and Y. Yanase, Locally non-centrosymmetric superconductivity in multilayer systems, *J. Phys. Soc. Jpn.* **81**, 034702 (2012).
- [21] S. Nakosai, Y. Tanaka, and N. Nagaosa, Topological Superconductivity in Bilayer Rashba System, *Phys. Rev. Lett.* **108**, 147003 (2012).
- [22] S. Khim, J. F. Landaeta, J. Banda, N. Bannor, M. Brando, P. M. R. Brydon, D. Hafner, R. Küchler, R. Cardoso-Gil, U. Stockert, A. P. Mackenzie, D. F. Agterberg, C. Geibel, and E. Hassinger, Field-induced transition within the superconducting state of  $\text{CeRh}_2\text{As}_2$ , *Science* **373**, 1012 (2021).
- [23] X. Zhang, Q. Liu, J.-W. Luo, A. J. Freeman, and A. Zunger, Hidden spin polarization in inversion-symmetric bulk crystals, *Nat. Phys.* **10**, 387 (2014).
- [24] C. Cheng, J.-T. Sun, X.-R. Chen, and S. Meng, Hidden spin polarization in the 1t-phase layered transition-metal dichalcogenides  $\text{MX}_2$  ( $M = \text{Zr}, \text{Hf}; X = \text{S}, \text{Se}, \text{Te}$ ), *Sci. Bull.* **63**, 85 (2018).
- [25] L. Yuan, Q. Liu, X. Zhang, J.-W. Luo, S.-S. Li, and A. Zunger, Uncovering and tailoring hidden Rashba spin-orbit splitting in centrosymmetric crystals, *Nat. Commun.* **10**, 906 (2019).
- [26] J. M. Riley, F. Mazzola, M. Dendzik, M. Michiardi, T. Takayama, L. Bawden, C. Granerød, M. Leandersson, T. Balasubramanian, M. Hoesch, T. K. Kim, H. Takagi, W. Meevasana, P. Hofmann, M. S. Bahramy, J. W. Wells, and P. D. C. King, Direct observation of spin-polarized bulk bands in an inversion-symmetric semiconductor, *Nat. Phys.* **10**, 835 (2014).
- [27] M. Gehlmann, I. Aguilera, G. Bihlmayer, E. Mlynczak, M. Eschbach, S. Döring, P. Gospodaric, S. Cramm, B. Kardynal, L. Plucinski, S. Blügel, and C. M. Schneider, Quasi 2D electronic states with high spin-polarization in centrosymmetric  $\text{MoS}_2$  bulk crystals, *Sci. Rep.* **6**, 26197 (2016).
- [28] D. Santos-Cottin, M. Casula, G. Lantz, Y. Klein, L. Petaccia, P. Le Fèvre, F. Bertran, E. Papalazarou, M. Marsi, and A. Gauzzi, Rashba coupling amplification by a staggered crystal field, *Nat. Commun.* **7**, 11258 (2016).
- [29] S.-L. Wu, K. Sumida, K. Miyamoto, K. Taguchi, T. Yoshikawa, A. Kimura, Y. Ueda, M. Arita, M. Nagao, S. Watauchi, I. Tanaka, and T. Okuda, Direct evidence of hidden local spin polarization in a centrosymmetric superconductor  $\text{LaO}_{0.55}\text{F}_{0.45}\text{BiS}_2$ , *Nat. Commun.* **8**, 1919 (2017).
- [30] W. Yao, E. Wang, H. Huang, K. Deng, M. Yan, K. Zhang, K. Miyamoto, T. Okuda, L. Li, Y. Wang, H. Gao, C. Liu, W. Duan, and S. Zhou, Direct observation of spin-layer locking by local Rashba effect in monolayer semiconducting  $\text{PtSe}_2$  film, *Nat. Commun.* **8**, 14216 (2017).
- [31] E. Razzoli, T. Jaouen, M.-L. Mottas, B. Hildebrand, G. Monney, A. Pisoni, S. Muff, M. Fanciulli, N. C. Plumb, V. A. Rogalev, V. N. Strocov, J. Mesot, M. Shi, J. H. Dil, H. Beck, and P. Aebi, Selective Probing of Hidden Spin-Polarized States in Inversion-Symmetric Bulk  $\text{MoS}_2$ , *Phys. Rev. Lett.* **118**, 086402 (2017).
- [32] N. Ghobadi and S. B. Touski, Structural, electrical and optical properties of bilayer  $\text{SiX}$  ( $X = \text{N}, \text{P}, \text{As}$  and  $\text{Sb}$ ), *J. Phys.: Condens. Matter* **33**, 285502 (2021).
- [33] J. Železný, H. Gao, K. Výborný, J. Zemen, J. Mašek, A. Manchon, J. Wunderlich, J. Sinova, and T. Jungwirth, Relativistic Néel-Order Fields Induced by Electrical Current in Antiferromagnets, *Phys. Rev. Lett.* **113**, 157201 (2014).
- [34] Y. Yanase, Magneto-electric effect in three-dimensional coupled zigzag chains, *J. Phys. Soc. Jpn.* **83**, 014703 (2014).
- [35] P. Wadley, B. Howells, J. Železný, C. Andrews, V. Hills, R. P. Campion, V. Novák, K. Olejník, F. Maccherozzi, S. S. Dhesi, S. Y. Martin, T. Wagner, J. Wunderlich, F. Freimuth, Y. Mokrousov, J. Kuneš, J. S. Chauhan, M. J. Grzybowski, A. W. Rushforth, K. W. Edmonds *et al.*, Electrical switching of an antiferromagnet, *Science* **351**, 587 (2016).
- [36] H. Watanabe and Y. Yanase, Symmetry analysis of current-induced switching of antiferromagnets, *Phys. Rev. B* **98**, 220412(R) (2018).
- [37] T. Jungwirth, X. Marti, P. Wadley, and J. Wunderlich, Antiferromagnetic spintronics, *Nat. Nanotechnol.* **11**, 231 (2016).
- [38] T. Koga, J. Nitta, H. Takayanagi, and S. Datta, Spin-Filter Device Based on the Rashba Effect Using a Nonmagnetic Resonant Tunneling Diode, *Phys. Rev. Lett.* **88**, 126601 (2002).
- [39] P.-Q. Jin and Y.-Q. Li, Magnification of the spin Hall effect in a bilayer electron gas, *Phys. Rev. B* **76**, 235311 (2007).
- [40] E. Bernardes, J. Schliemann, M. Lee, J. C. Egues, and D. Loss, Spin-Orbit Interaction in Symmetric Wells with Two Subbands, *Phys. Rev. Lett.* **99**, 076603 (2007).
- [41] R. S. Calsaverini, E. Bernardes, J. C. Egues, and D. Loss, Intersubband-induced spin-orbit interaction in quantum wells, *Phys. Rev. B* **78**, 155313 (2008).
- [42] M. Akabori, S. Hidaka, H. Iwase, S. Yamada, and U. Ekenberg, Realization of  $\text{In}_{0.75}\text{Ga}_{0.25}\text{As}$  two-dimensional electron gas bilayer system for spintronics devices based on Rashba spin-orbit interaction, *J. Appl. Phys.* **112**, 113711 (2012).



- [43] F. G. G. Hernandez, L. M. Nunes, G. M. Gusev, and A. K. Bakarov, Observation of the intrinsic spin Hall effect in a two-dimensional electron gas, *Phys. Rev. B* **88**, 161305(R) (2013).
- [44] S. Souma, A. Sawada, H. Chen, Y. Sekine, M. Eto, and T. Koga, Spin Blocker Using the Interband Rashba Effect in Symmetric Double Quantum Wells, *Phys. Rev. Appl.* **4**, 034010 (2015).
- [45] A. Khaetskii and J. C. Egues, Giant edge spin accumulation in a symmetric quantum well with two subbands, *Europhys. Lett.* **118**, 57006 (2017).
- [46] K. Hayashida and H. Akera, D'yakonov-perel' spin relaxation in a bilayer with local structural inversion asymmetry, *Phys. Rev. B* **101**, 035306 (2020).
- [47] F. J. Ohkawa and Y. Uemura, Quantized surface states of a narrow-gap semiconductor, *J. Phys. Soc. Jpn.* **37**, 1325 (1974).
- [48] Y. A. Bychkov and E. I. Rashba, Oscillatory effects and the magnetic susceptibility of carriers in inversion layers, *J. Phys. C* **17**, 6039 (1984).
- [49] Y. A. Bychkov and E. I. Rashba, Properties of a 2D electron gas with lifted spectral degeneracy, *JETP Lett.* **39**, 78 (1984).
- [50] S. Faniel, T. Matsuura, S. Mineshige, Y. Sekine, and T. Koga, Determination of spin-orbit coefficients in semiconductor quantum wells, *Phys. Rev. B* **83**, 115309 (2011).
- [51] H. Akera, H. Suzuura, and Y. Egami, Gate-voltage-induced switching of the Rashba spin-orbit interaction in a composition-adjusted quantum well, *Phys. Rev. B* **95**, 045301 (2017).
- [52] T. Ishikawa and H. Akera, Antiparallel spin Hall current in a bilayer with skew scattering, *Phys. Rev. B* **100**, 125307 (2019).
- [53] T. Ishikawa and H. Akera, Ac response of spin-pseudospin current in a double quantum well, *Jpn. J. Appl. Phys.* **61**, 063002 (2022).
- [54] G. S. Boebinger, H. W. Jiang, L. N. Pfeiffer, and K. W. West, Magnetic-Field-Driven Destruction of Quantum Hall States in a Double Quantum Well, *Phys. Rev. Lett.* **64**, 1793 (1990).
- [55] S. Q. Murphy, J. P. Eisenstein, G. S. Boebinger, L. N. Pfeiffer, and K. W. West, Many-Body Integer Quantum Hall Effect: Evidence for New Phase Transitions, *Phys. Rev. Lett.* **72**, 728 (1994).
- [56] A. A. Bykov, D. R. Islamov, A. V. Goran, and A. I. Toropov, Microwave photoresistance of a double quantum well at high filling factors, *JETP Lett.* **87**, 477 (2008).
- [57] M. I. Dyakonov and V. I. Perel, Possibility of orienting electron spins with current, *Sov. Phys. JETP* **13**, 467 (1971).
- [58] M. I. Dyakonov and V. I. Perel, Current-induced spin orientation of electrons in semiconductors, *Phys. Lett. A* **35**, 459 (1971).
- [59] S. Murakami, N. Nagaosa, and S.-C. Zhang, Dissipationless quantum spin current at room temperature, *Science* **301**, 1348 (2003).
- [60] J. Sinova, D. Culcer, Q. Niu, N. A. Sinitsyn, T. Jungwirth, and A. H. MacDonald, Universal Intrinsic Spin Hall Effect, *Phys. Rev. Lett.* **92**, 126603 (2004).
- [61] Y. K. Kato, R. C. Myers, A. C. Gossard, and D. D. Awschalom, Observation of the spin Hall effect in semiconductors, *Science* **306**, 1910 (2004).